N-Heterocyclic carbene-functionalized magic number gold nanoclusters

Mina R. Narouz[1], Kimberly M. Osten[1], Phillip J. Unsworth[1], Renee W.Y. Man[2], Kirsi Salorinne[2], Shinjiro Takano[3], Ryohei Tomihara[3], Sami Kaappa[4], Sami Malola[4], Cao-Thang Dinh[5], J. Daniel Padmos[1], Kennedy Ayoo[1], Patrick J. Garrett[1], Masakazu Nambo[2], J. Hugh Horton[1], Edward H. Sargent[5], Hannu Häkkinen*[4], Tatsuya Tsukuda*[3,6], Cathleen M. Crudden*[1,2]

Magic number metal nanoclusters are atomically precise nanomaterials that have enabled unprecedented insight into structure-property relationships in nanoscience. Thiolates are the most common ligand, binding to the cluster via a staple motif in which only central gold atoms are in the metallic state. The lack of other strongly-bound ligands for nanoclusters with different bonding modes has been a significant limitation in the field. Herein, we report a previously unknown ligand for gold (0) nanoclusters: *N*-heterocyclic carbenes (NHCs), which feature a robust metal-carbon single bond, and impart high stability to the corresponding gold cluster. The addition of a single NHC to gold nanoclusters results in significantly improved stability and catalytic properties in the electrocatalytic reduction of CO_2. By varying the conditions, nature and number of equivalents of the NHC, predominantly or exclusively monosubstituted NHC-functionalized clusters result. Clusters can also be obtained with up to five NHCs, as a mixture of species.

Magic number metal nanoclusters stabilized by organic ligands are intriguing species that bridge the gap between molecules and materials.[1-3] Although clearly nanomaterials, with size dependent properties, they can be described with a single molecular formula, have discrete electronic transitions due to well-defined molecular orbitals and can be characterized by techniques usually employed in molecular science. Kornberg and co-workers' determination of the precise structure of the cluster $Au_{102}(SR)_{44}$ using single crystal X-ray diffraction was a watershed moment in the understanding of these nanomaterials.[4] The crystallographically-determined structure partially confirmed earlier computational predictions on the bonding at the gold-thiolate interface and provided strong support for the "superatom" theory of closed electronic shells, first described by Häkkinen et al. to explain why certain cluster sizes are over represented among known species, and hence "magic".[2,5]

Since this seminal paper by Kornberg, research into magic number nanoclusters featuring different thiolates, metals, core configurations and applications has abounded.[6-10] However, with few exceptions, thiols and phosphines remain virtually the only organic ligands employed to stabilize these structures, along with some work on alkynes.[11-17]

N-heterocyclic carbenes (NHCs) are phosphine analogues that have attracted considerable attention in organometallic chemistry, and recently in surface science.[18-30] In organometallics, these ligands are known for their ability to form strong, substitutionally inert bonds to various metals.[31,32] Recently they have been shown to form highly robust self-assembled monolayers (SAMs) on Au(111) surfaces and nanoparticles,[20] however their use as stabilizing ligands in magic number nanoclusters has not been previously described. NHCs have, however been described as stabilizing ligands in small, mixed valency clusters of 3-4 atoms in seminal work by the Corrigan[33,34] and Sadighi groups.[35,36]

Herein we report the first example of NHC-stabilized Au (0) nanoclusters.[33,34,35] Au_{11} nanoclusters functionalized by up to five NHC ligands have been prepared and characterized. Remarkably, the addition of even one NHC to the Au_{11} cluster significantly increases the thermal stability of this important nanocluster and improves its activity in the electrochemical reduction of CO_2 to CO, which is a critically important reaction in the valorization of CO_2.

Results and discussion

Development of cluster synthesis. Our studies began with preformed phosphine-stabilized undecagold clusters $Au_{11}(PPh_3)_7Cl_3$ and $[Au_{11}(PPh_3)_8Cl_2]Cl$.[37] Phosphine-stabilized clusters were chosen since NHC and phosphine ligands are both neutral and thus require no change in oxidation state or cluster charge to accompany an exchange reaction. Furthermore,

[1]Department of Chemistry, Queen's University, Chernoff Hall, Kingston, Ontario K7L 3N6 Canada [2]Institute of Transformative Bio-Molecules (WPI-ITbM), Nagoya University, Nagoya, 464-8601, Japan [3]Department of Chemistry, School of Science, The University of Tokyo, 7-3-1 Hongo, Bunkyo-ku, Tokyo 113-0033, Japan [4]Departments of Chemistry and Physics, Nanoscience Center, University of Jyväskylä, 40014 Jyväskylä, Finland [5]Department of Electrical and Computer Engineering, The University of Toronto, Toronto, Ontario M5S 3G4, Canada [6]Elements Strategy Initiative for Catalysts and Batteries (ESICB), Kyoto University, Katsura, Kyoto 615-8520, Japan

phosphine-stabilized clusters do not have a layer of Au(I) atoms on the exterior, as is the case for thiolate-stabilized clusters.

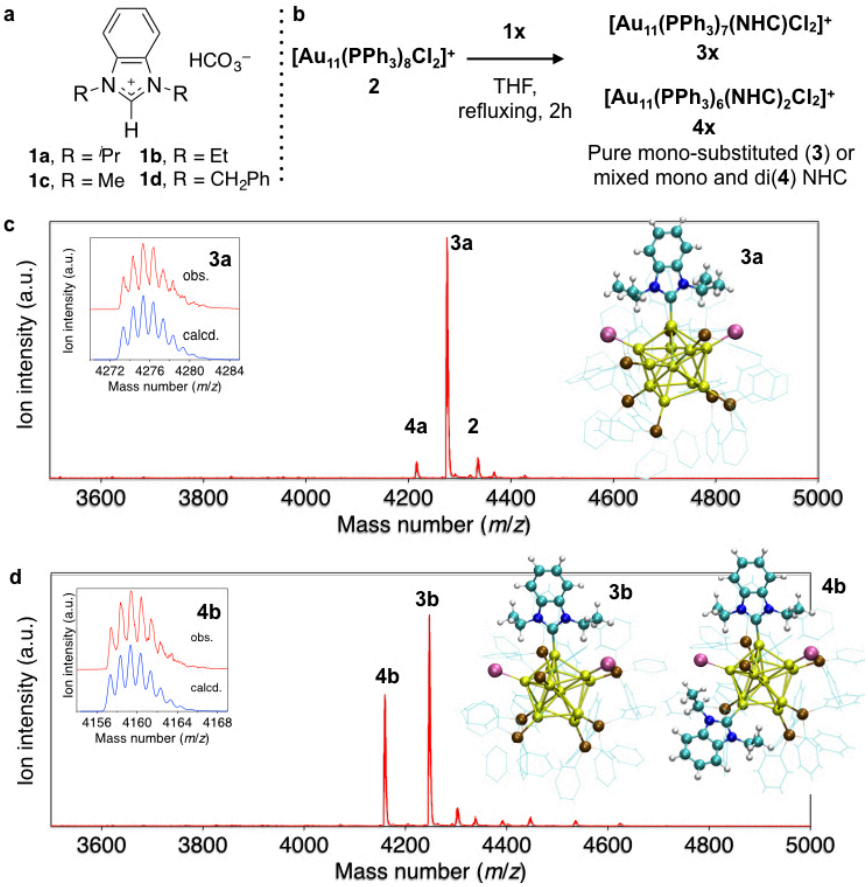

Figure 1 | Synthesis and characterization of NHC-modified Au_{11} nanoclusters. a, Structure of *N*-heterocyclic carbene (NHC) precursors employed in this study featuring a variety of organic substituents on the nitrogen atoms flanking the key carbon. **b**, Reaction of undecagold cluster $[Au_{11}(PPh_3)_8Cl_2]Cl$ (**2**) with NHC precursors from panel **a** resulting in formation of new NHC-containing clusters. **c**, Mass spectroscopic characterization of the reaction mixture leading to $[Au_{11}(PPh_3)_7(NHC^{iPr})Cl_2]Cl$ **3a**, along with structure obtained by X-ray crystallography. Observed vs. calculated isotope pattern is shown in the inset. The high level of purity is notable from the mass spectrum, which shows **3a** as the major product, along with small quantities of starting cluster **2** and di-substituted cluster $[Au_{11}(PPh_3)_6(NHC^{iPr})_2Cl_2]Cl$ **4a**. Colours in the atomistic structures: yellow: Au; purple: Cl; brown: P; blue: N, cyan: C; white: H. **d**, Mass spectroscopic characterization of the reaction of **1b** with **2**, showing a mixture of **3b** and **4b** along with DFT-predicted structures. Note that the structure of **3a** shown in **c** is an actual crystal structure while **3b** and **4b** are DFT-simulated.

Treatment of $[Au_{11}(PPh_3)_8Cl_2]Cl$ (**2**) with di-isopropyl benzimidazolium hydrogen carbonate **1a** (Fig. 1a) in THF at 66 °C gave predominantly a single NHC-containing cluster (**3a**, Table 1, entry 1). This cluster results from substitution of one phosphine ligand for the NHC (Fig. 1b). The less stable cluster $Au_{11}(PPh_3)_7Cl_3$ was considerably less effective.

Conclusive information about the cluster identity was obtained by mass spectrometry, which demonstrated that mono-substituted cluster **3a** is the predominant product, accompanied by small amounts of disubstituted cluster **4a** and starting material **2** (Fig. 1c). Quantification of the cluster purity was accomplished by detailed ^{1}H NMR analysis. For precise details and replicate runs, the reader is referred to SI section 2. NHC nanoclusters were analyzed before and after purification by chromatography on silica gel, which indicated that there was no change in the cluster distribution after chromatography, and highlighted the stability of the cluster to chromatography (Fig. S33). The main effect of purification was to remove molecular by-products such as $[Au(NHC)_2]^+$ and $OPPh_3$ (Fig. S12).

Increasing the amount of **1a** to 5 equivalents resulted in larger amounts of the disubstituted cluster **4a**, with the addition of water attenuating reactivity and giving a more selective process (Table 1, entries 2 and 3). The use of the free NHC in place of the bicarbonate salt gave similar overall yields, but a mixture of clusters was obtained (entry 4). The monosubstituted cluster **3a** still predominated, but disubstituted cluster **4a** was now observed along with trisubstituted cluster **5a**. ESI-MS revealed the presence of trace amounts of the tetra- and penta-substituted clusters **6a** and **7a**. Thus, the use of the bicarbonate salt **1a** at approximately 1 equivalent is important to produce clusters which are predominantly mono-substituted.

With conditions in hand for the preparation of NHC-stabilized clusters **3a** and **4a**, we then examined the effect of NHC structure (Table 1). NHC precursors **1b**-**d** were employed, where the nitrogen atoms of the NHC are substituted with Et, Me and Bn groups. Each of these relatively minor changes in NHC structure had an influence on the reaction. NHC precursor **1b** (R = Et) consistently gave a mixture of mono and di-substituted clusters regardless of conditions or stoichiometry, suggesting that the initial substitution activates the cluster for a second displacement reaction (Fig. 1d and Table 1, entries 5-8). Again, increasing the amount of the NHC gave greater substitution (see SI section 2).

Table 1 | Reaction conditions for preparation of NHC-stabilized clusters

$[Au_{11}(PPh_3)_8Cl_2]^+$ —1x, conditions→ $[Au_{11}(PPh_3)_{8-n}(NHC)_nCl_2]^+$

Entry	1x (equiv.)	Additive	Cluster(s) produced[a]	Yield[b] (%)
1	**1a** (1.2)	None	**3a**,**4a** (9:1)	22[c]
2	**1a** (5.0)	H_2O[d]	**3a**,**4a** (3:1)	26[c]
3	**1a** (5.0)	None	**3a**,**4a** (1:1)	38
4	**1a** (1.2)[e]	None	**3a**,**4a**,**5a** (2.6:1:1)	24
5	**1b** (1.2)	H_2O	**3b**,**4b** (2:1)	41
6	**1b** (1.2)	None	**3b**,**4b** (2:1)	20
7	**1b** (5.0)	H_2O	**3b**,**4b** (1:1)	64
8	**1b** (5.0)	None	**3b**,**4b** (1:1)	43
9	**1c** (1.2)	H_2O	**3c**	6[c]
10	**1c** (1.2)	H_2O[f]	**3c**	10[c]
11	**1d** (1.2)	None	**3d**,**4d**,**5d**[g]	18
12	**1d** (9.0)	None	**3d**,**4d**,**5d**,**6d**[g]	38

[a]Conditions: THF solvent, 70 °C, 2h. **3x** clusters contain 1 NHC (n=1), **4x** (n=2), **5x** (n=3), **6x**, (n=4), ratios determined by ^{1}H NMR spectroscopy, traces of starting cluster **2** present in some cases; [b]Isolated yields; [c]Average of 3-5 runs; [d]Water added at 500 ppm unless otherwise noted; [e]Free carbene employed; [f]40 °C, 1000 ppm H_2O; [g]Exact ratios difficult to elucidate by NMR. ESI-MS analysis shows decreasing amounts of more substituted clusters.

NHC precursor **1c** (R = Me) behaved more like **1a** and allowed for the isolation of clean, mono-substituted cluster **3c** with no evidence for formation of the di-substituted clusters **4c** under optimized conditions. On average, lower yields isolated were observed by comparison to reactions with **1a** and **1b**, and the reaction was best run at lower temperatures (Table 1, entries 9 and 10). The addition of larger quantities of this small NHC gave cluster degradation rather than increased substitution (see SI sections 2 and 3).

Finally, benzylated NHC precursor (**1d**) behaved similarly to **1b**, giving a mixture of mono and di-substituted clusters **3d** and **4d** even at 1.2 equivalents of the precursor. At higher loadings (9.0 equiv.), a mixture of clusters including mono- (**3d**), di- (**4d**), tri- (**5d**) and tetra- (**6d**) NHC-containing clusters was observed (Table 1, entries 11 and 12 and Figs. S45-48).

Computational studies and structure prediction. Density functional theory (DFT-implemented as described in reference (38) for technical details see Supplementary Information) was employed to investigate the energetics of substitution of the various phosphines in cluster **2** by NHCs (Fig. 2a). Introduction of NHC (**1a**) into cluster **2** was found to be thermodynamically favorable at most sites, with the exception of phosphine **8** (P8), which gave an unfavourable reaction energy change of +0.05 eV, likely due to steric constraints at this site (Fig. 2b). Introduction of the NHC by displacement of phosphines adjacent to the Au–Cl sites was uniformly preferred, with the single most favourable exchange predicted to occur at P2 for all NHCs examined. Differences between exchange at P2 and the next favourable phosphine energetically were 0.18 eV, 0.07 eV, and 0.06 eV for **3a**, **3b** and **3c**, respectively (Fig. 2b and Table S7). The calculated HOMO–LUMO gaps for the mono-substituted clusters were largest for substitution at P2 for each NHC type, showing that the trends in electronic stability followed exchange energetics (Table S8).

For the reaction of NHC precursor **1b** with **2** to form di-substituted clusters, the four lowest-energy isomers were found within a 0.1 eV window. Three of these included introduction of the NHC at P2 (Table S9). NHC precursors **1a** and **1c** were also predicted to have favourable energetics for the production of disubstituted clusters. For example, substitution of **1a** and **1c** at P2 and P7 led to energy changes of −1.39 eV and −1.43 eV respectively, suggesting that kinetic control rather than thermodynamics must play a role in the observation of predominantly or exclusively monosubstitution for these NHCs.

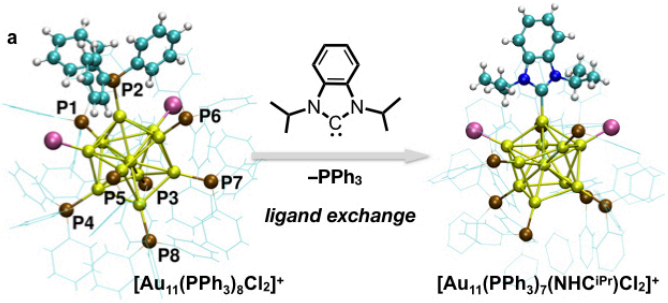

b

Phosphine	Energy (eV)[a]
P1	−0.64
P2	**−0.93**
P3	−0.73
P4	−0.55
P5	−0.41
P6	−0.40
P7	−0.75
P8	+0.05

[a]Changes in potential energy for reaction of **2** with **3a** by DFT.

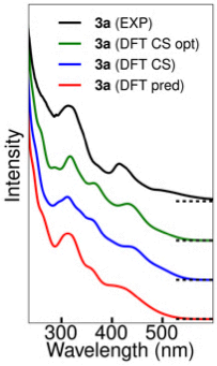

Figure 2 | DFT and UV-visible spectroscopic prediction of structure for NHC-modified nanoclusters. a, Labelling of phosphines in $[Au_{11}(PPh_3)_8Cl_2]Cl$ (**2**) and exchange with **1a**. **b**, DFT-predicted changes in potential energy for reaction shown in panel **a** at each phosphine. **c**, comparison of calculated optical spectra (red, blue, green curves) of cluster **3a** to experimental data (black). The three computed spectra are calculated for the initial DFT-predicted structure obtained by replacing phosphine P2 in cluster **2** by NHC (red), for the crystal structure as such (blue), and for the DFT-optimized crystal structure (green). The computed spectra are blue-shifted by 0.4 eV for better visual comparison to the experimental data.

In the later stages of this work, we were able to determine the atomistic structure of **3a** from a single crystal X-ray analysis (*vide subra*). The crystal structure

confirmed our DFT predictions that it is energetically optimal to replace phosphine P2 by an NHC in cluster **3a** (see the comparison of the predicted and observed structures in Figure S52). Three computational structure models for **3a** were now at our hands, one based on the predicted structure mentioned above, one taking the crystal structure as such, and one obtained from the crystal structure by DFT optimization.

The computed optical absorption spectra from these models are compared to the experimental data measured for **3a** in Fig. 2c. We notice that all computed spectra have spectral features that match the experimental data very well, however the computed spectra were underestimating systematically all transition energies by about 0.4 eV. This is understandable based on the properties of the DFT functional used in the calculation. The shift is corrected in Figure 2c to enable a better visual comparison to experiment. The nature of the dominant two absorption features in the computed spectra (close to 300 nm and 450 nm in the shifted spectra) are further analyzed in Figure S53. The dominant transitions were found to be either from Au s-type (450 nm) or Au d-type (300 nm) states to the empty states of the phenyl rings of the phosphines.

Spectroscopic characterization. The clusters were also extensively characterized by nuclear magnetic resonance (NMR) spectroscopy, examining ^{1}H, ^{31}P and ^{13}C nuclei (see SI section 3). The NHC carbon bound to Au could not be observed by ^{13}C NMR at natural abundance, but when cluster **3a** was prepared with ^{13}C enrichment at C2 of the NHC, the Au–C bond could be observed at 209 ppm. This signal appeared as an octet, indicating equivalent coupling to each of the seven phosphines (Fig. 3a). Since there are at least two unique environments for phosphines in any NHC-containing cluster, exchange processes must be happening on the time scale of the NMR experiment. ^{31}P NMR spectroscopy supports the presence of exchange phenomena at room temperature since a clean singlet was observed (Fig. 3b). To address this further, low temperature ^{31}P NMR spectra were obtained for both **2** and **3a**, (see SI Figs. S50 and S51). These spectra confirm the presence of exchange phenomenon/a on the NMR time scale. Interestingly, the NHC-functionalized cluster starts to show decoalescence at –10 °C, while the all phosphine cluster **2** does not begin to decoalesce until close to –70 °C.

Information on the bonding and electronic properties of the clusters was also obtained through Au L_3-edge X-ray absorption spectroscopy (XAS). X-ray absorption near edge structure (XANES) spectra show a decrease in intensity when the NHC is introduced into the clusters (Fig. S56), particularly for the Me derivative **3c**, which may be due to the electron-donating ability of NHCs.[32,39,40]

Extended X-ray absorption fine structure (EXAFS) *R*-space spectra of the clusters revealed information on Au–C, Au–P and Au–Cl bonding, and Au-Au bonding within the cluster (Fig. S55 and Table S10). Analysis of Au–C bond lengths revealed that the Au–C(NHC) bond length in **3c** is 11.4 pm shorter than the corresponding Au–C bond in **3a**, consistent with steric differences between the NHC types. Most importantly, the introduction of NHC **1a** resulted in a 3 pm increase in the average Au–Au bond length for gold atoms on the exterior of the cluster, relative to the all phosphine cluster **2**, which suggests that NHC ligation leads to expansion of the outermost Au atoms in the cluster. A similar cluster expansion was not observed upon ligation of smaller NHC in cluster **3c**, which is interesting considering that this cluster has higher stability than **3a** (*vide infra*), suggesting an interplay between experimental observations of cluster structure and stability.

The longer Au–C bond and its effect on the underlying structure has precedent in DFT studies, which propose that binding of an NHC results in restructuring of the surface Au atoms in Au(111) systems,[20,41,42] however this effect has been difficult to observe experimentally. Thus, the EXAFS results reported herein represent the first direct measurement of the NHC influence on underlying structure in metallic Au materials.

DFT calculations supported the trends observed experimentally by EXAFS. When the bond lengths were averaged over each of the optimized clusters, DFT studies predicted a 1.9 pm shorter Au-C bond in **3c** compared to **3a**. Similarly, the averaged calculated Au-Au bond length for the exterior gold atoms increased 1.0 pm for the **3a** cluster compared to **2** while cluster **3c** showed no core expansion within error.

Single crystal X-ray diffraction study of nanocluster 3a. X-ray quality single crystals of **3a** were grown by layering of *n*-hexane onto a solution of **3a** in dichloromethane at room temperature. After several days, reddish prisms of **3a** could be observed. Since dichloromethane co-crystallizes with **3a**, degradation of the crystal was observed upon drying. The structure of the cluster obtained from this study was found to be the same as that predicted by DFT, namely resulting from displacement of P2 (Fig. 3c). Although static disorder in the region of the NHC ligand complicates a detailed analysis of the Au–C bond length, the value obtained (2.09(2) Å) is in the same range as that predicted by EXAFS analysis (2.161(6) Å, Table S10). Taken in aggregate, the Au–Au bonds in the cluster were seen to contract upon introduction of the NHC ligand, however localized bonds experience contractions and expansions that may be significant for catalysis (see SI Figs. S57, S58, Tables S11 and Table S12).

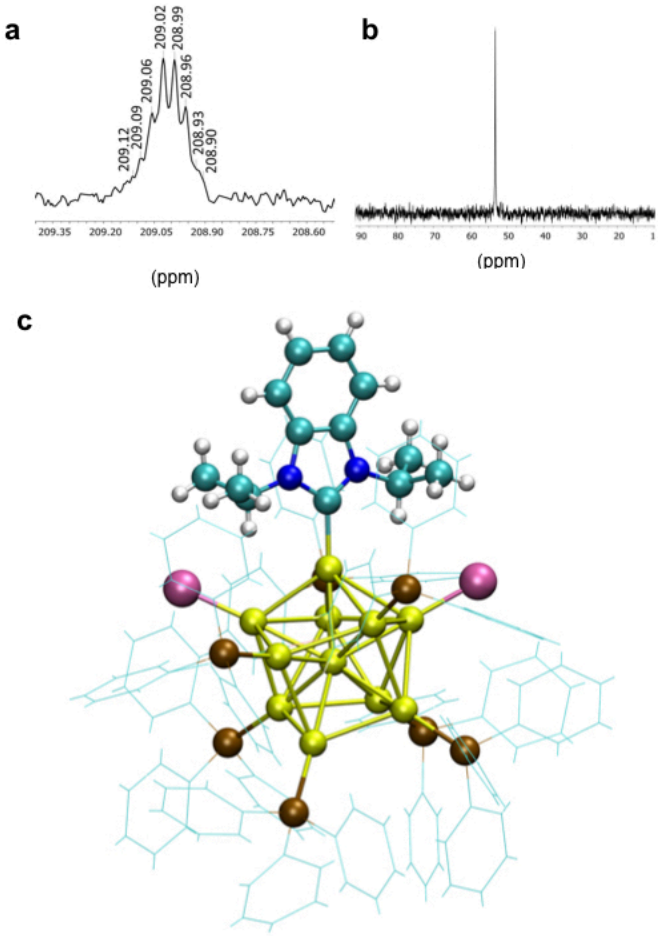

Figure 3 | Spectroscopic and X-ray diffraction characterization of NHC-substituted cluster **3a**. **a**, ^{13}C nuclear magnetic resonance (NMR) spectrum of **3a** bearing ^{13}C-labeled NHC, which enables identification of Au–C resonance. The signal appears as an octet from equal coupling to all seven phosphines. **b**, ^{31}P NMR spectrum showing a single resonance at room temperature consistent with rapid exchange. **c**, Single crystal X-ray diffraction structure for NHC cluster **3a** showing NHC incorporation at P2 as proposed from DFT studies.

Stability and catalytic activity of nanoclusters. Stability and ligand dissociation were also assessed using collision-induced dissociation (CID) mass spectrometry. In Figure 4, we compare the in-source CID mass spectra of **2** and **3a**, recorded under identical conditions. Cluster **2** undergoes loss of $Au(PPh_3)Cl$ and PPh_3 as major CID paths (Fig. 4a). In contrast, loss of the $Au(NHC^{iPr})Cl$ unit was the most dominant CID pathway for **3a** (Fig. 4b), even though the ratio of NHC^{iPr} to PPh_3 in the cluster is 1:7. In addition, direct dissociation of the NHC^{iPr} ligand by Au–C bond cleavage was not observed under any conditions, in sharp contrast to **2**, where the loss of PPh_3 was observed. These results suggest that NHC^{iPr} has significantly higher binding affinity to Au than PPh_3 does. These conclusions were supported by TGA-MS data, which also showed that phosphines are the first ligands to be lost (Table S13, Figs. S61-64).

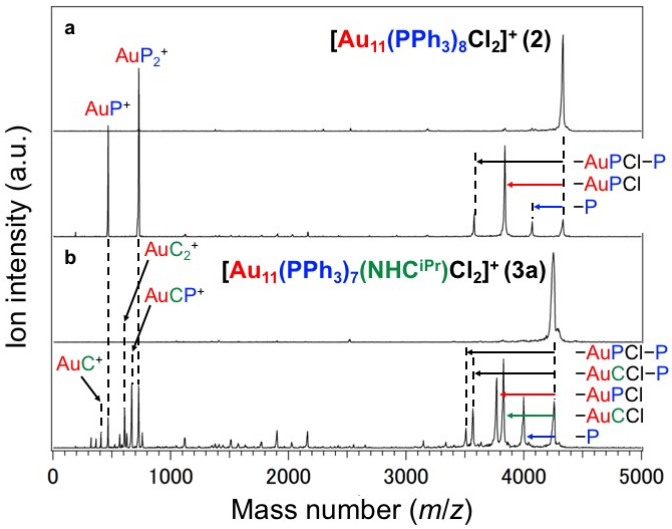

Figure 4 | In-source CID mass spectra of **2** (panel **a**) and **3a** (panel **b**). Upper and lower spectra of each panel were recorded at the CID voltage of 0 V and 200 V, respectively. Notations C and P represent NHC^{iPr} and PPh_3, respectively.

Thermal stability of the clusters was assessed by heating clusters in various solvents and monitoring the molecular transitions by UV-vis spectroscopy. The all phosphine cluster **2** was employed as a benchmark, which underwent complete decomposition after heating to 70°C in pentanol (12 h) and toluene at 70°C (24h). By contrast, NHC-stabilized clusters showed dramatically improved stability, with **3c** displaying virtually no change over 24 h at 70°C in toluene, (Fig. S59). Stability was reduced in the polar solvent pentanol, which allowed us to differentiate between the different NHC-functionalizaed clusters (Figs. 5a/b and Fig. S60). Among the clusters examined, cluster stability tracked with sterics, with **3c** being the most stable, showing virtually no decomposition after 12 h at 70 °C in pentanol (Figs. 5a and b). Clusters **2**, **3a** and **3b** change colour from yellow (clusters) to purple (nanoparticles) after heating in pentanol (Figure 5). The relative stability of the clusters is thus **2**<**3a**<**3b**<**3c**. TGA-MS studies also showed that **3c** was the most stable of all clusters, with onset of ligand loss occurring 15–20 °C higher than all other clusters (Figs. S61-64).

With a detailed understanding of structure and stability in hand, we examined these clusters as catalysts for the electrocatalytic reduction of CO_2 to CO (Fig. 5c).[43-48] This is an important reaction since CO is the key component in many high-volume carbon–carbon bond-forming reactions such as the oxo reaction and the Cativa process.

Nanoclusters **2**, **3a** and **3c** were dissolved in a mixture of isopropanol and toluene (1:2 v/v) and deposited on

carbon paper electrodes with a catalyst loading of 0.25 mg/cm^2. The electrodes were then dried at room temperature before activating in air by heating to 180°C for 2 h. This temperature was coincident with changes in the TGA of the nanoclusters that are attributed to loss of a phosphine ligand (Table S13 and Figs. S61-64). Lower temperatures resulted in significantly lower activity and longer treatment (6h) at 180 °C was also detrimental (Fig. S67).

Electroreduction of CO_2 was performed using a three-electrode system, with Pt mesh used as reference and counter electrodes, which were submerged in a CO_2–saturated, 0.1 M $KHCO_3$ electrolyte solution. During the reaction, CO_2 was introduced by bubbling the gas through the electrolyte at 15 standard cubic centimeters per minute, and the product gases were analyzed by gas chromatography.

As shown in Fig. 5c, nanocluster **3c** outperformed all phosphine cluster **2** and cluster **3a** bearing an isopropylated NHC. Nanocluster **3c** affected the electrocatalytic CO_2 reduction with the highest Faradaic efficiency (selectivity for CO production vs. H_2). Similarly, cluster **3c** had the highest current density (mA/cm^2) and mass activity (A/g) of all clusters tested, at all voltages employed (Fig. 5c), with the greatest differences being observed at -1.0 V (vs RHE). Higher loadings of this nanocluster on the surface led to decreased performance, suggesting that more highly dispersed nanoclusters are more active than any agglomerated species that may form (Fig. S68).

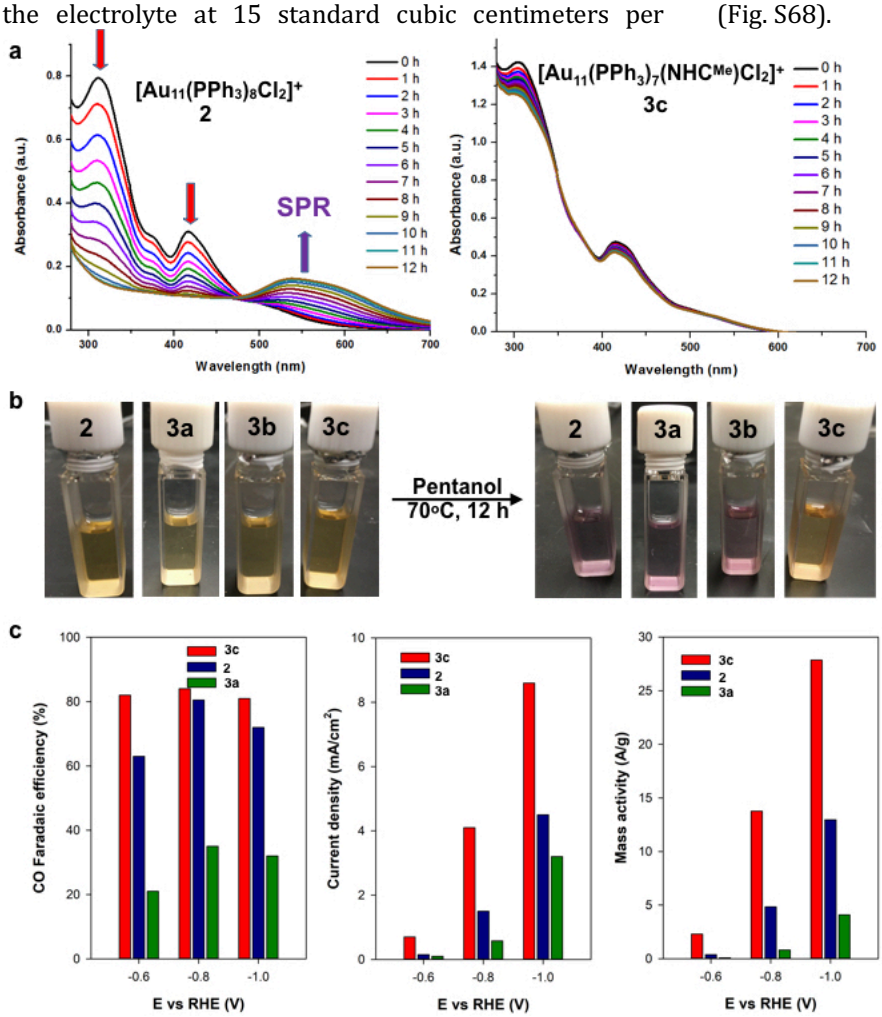

Figure 5 | Nanocluster stability and activity in the electrocatalytic reduction of CO_2 to CO. a, UV-Visible spectra of clusters **2** and **3c** in pentanol at 70°C over 12 hours. Cluster **2** decomposes to nanoparticles, evident by the loss of molecular signals at 405 and 310 nm and growth of the signal at 550 nm while **3c** is completely stable. **b**, Nanoclusters **2**, **3a**, and **3c** before and after thermal treatment showing the decomposition of **2** and **3a**, while nanocluster **3c** remains intact. **c**, Catalytic activity and selectivity of nanoclusters **2**, **3a** and **3c** in the CO_2 to CO reduction showing that nanocluster **3c** has the highest Faradaic efficiency for CO, the highest current density and the highest mass activity among the nanoclusters tested. While Faradaic efficiency seems independent of applied current, catalytic activity (as assessed through current density and mass activity) is highest at –1.0 V (vs. RHE).

Compared with related NHC-functionalized nanoparticles reported by Chang and Yang, nanocluster **3c** displays similar levels of Faradaic efficiency and current density, although at more negative voltages.[44,45] The best nanostructured catalysts in the literature again give similar results, but at lower overpotentials, as a consequence of high catalyst loadings.[44,48] With the high mass activity already observed for **3c**, performance improvements would be expected by the use of higher surface area supports such as carbon nanoparticles.[44]

To ensure that CO_2 is the source of the observed CO, the reaction was carried out with ^{13}C-labelled CO_2. Analysis of this reaction by GC-MS analysis (Fig. S66) shows clear incorporation of the isotope into carbon monoxide (^{13}CO,

m/z =29), confirming that the CO is produced from CO_2 by comparison with CO obtained from $^{12}CO_2$ where GC analysis gave an m/z of 28 mass units for ^{12}CO. Only trace amounts of formate were observed upon prolonged exposure (1%) illustrating the high selectivity of the reaction (Fig. S69).

Interestingly, cluster **3c** is the only cluster of those examined that retained its structure and did not decompose to nanoparticles upon extended thermal treatment. This observation leads to the intriguing possibility that having an intact nanocluster is important for catalytic activity, and illustrates the advantage of employing molecular species such as clusters as catalysts. It should be noted that NHC substitution does not uniformly lead to improved catalysts since cluster **3a** was outperformed by all-phosphine cluster **2**. Although the precise reasons for this difference are not presently clear, it may be that comparisons across cluster types are not as valid as comparisons within the NHC series **3a, b** and **c**. However, it is clear that the most stable cluster examined (**3c**) also gives the highest activity.

Conclusion

In conclusion, we have reported the first example of the use of NHCs to stabilize gold (0) nanoclusters. The introduction of the NHC can be accomplished by a simple displacement reaction employing benzimidazolium carbonate salts. The number of NHCs introduced is controllable by NHC structure, equivalents and reaction conditions. The structures of the NHC-containing clusters were predicted by DFT and confirmed by a combination of mass spectrometry, NMR, EXAFS, XANES, UV-Vis spectroscopy, and single crystal XRD. The stability of the NHC-containing clusters was assessed by treatment at high temperature in a variety of solvents and by CID mass spectrometry and TGA-MS. NHC-containing clusters were found to be more stable than the all phosphine clusters, with absolute stability dictated by the nature of the NHC. The performance of various clusters in electrocatalytic CO_2 reduction was found to correlate with cluster stability, with the most stable cluster having the highest Faradaic efficiency, catalytic activity and current density. These observations suggest that these novel NHC-stabilized gold clusters can have quantifiable benefits on electrocatalytic performance, which can be enhanced even further due to an atomically precise understanding of their structure.

Methods

In a two-neck flask equipped with a condenser and an argon balloon, a mixture of $[Au_{11}(PPh_3)_8Cl_2]Cl$ (**2**) and the corresponding benzimidazolium hydrogen carbonate (**1x**) were dissolved in in THF (1 mL of THF per 1 mg of **2**). The resulting mixture was heated at 70°C for 2 h before cooled to room temperature. The solvent was removed *in vacuo* to give an orange solid, which was dissolved in dichloromethane (DCM) and passed through a Celite plug to remove any insoluble orange particles. The solvent was evaporated under an air stream and the resulting orange solid was triturated with Et_2O (2 × 5 mL) to remove triphenylphosphine oxide. The resulting clusters were dissolved in a minimum amount of DCM to give a red solution which was loaded onto a silica gel column packed with DCM/MeOH (25:1 v/v). The product was eluted with DCM/MeOH (9:1) to give the desired cluster as a red solid after solvent evaporation *in vacuo*. For details of specific experiments, the reader is referred to the supplementary information.

Data availability

Spectral and purity data are available for all new compounds, along with original NMR, MS, XPS, UV-vis DFT, TGA–MS and electrochemical data. Single crystal X-ray crystallographic data are included for cluster **3a**. All data described in the manuscript are available in the supplementary information or from the authors upon request.

References

1 Bürgi, T. Properties of the gold-sulphur interface: From self-assembled monolayers to clusters. *Nanoscale* **7**, 15553-15567 (2015).

2 Häkkinen, H. The gold–sulfur interface at the nanoscale. *Nat. Chem.* **4**, 443 (2012).

3 Yamazoe, S., Koyasu, K. & Tsukuda, T. Nonscalable oxidation catalysis of gold clusters. *Acc. Chem. Res.* **47**, 816–824 (2014).

4 Jadzinsky, P. D., Calero, G., Ackerson, C. J., Bushnell, D. A. & Kornberg, R. D. Structure of a thiol monolayer-protected gold nanoparticle at 1.1 Å resolution. *Science* **318**, 430-433 (2007).

5 Häkkinen, H., Walter, M. & Grönbeck, H. Divide and protect: Capping gold nanoclusters with molecular gold-thiolate rings. *J. Phys. Chem. B* **110**, 9927-9931 (2006).

6 Qian, H., Zhu, M., Wu, Z. & Jin, R. Quantum sized gold nanoclusters with atomic precision. *Acc. Chem. Res.* **45**, 1470-1479 (2012).

7 Hesari, M., Workentin, M. S. & Ding, Z. NIR electrochemiluminescence from Au_{25}^- nanoclusters facilitated by highly oxidizing and reducing co-reactant radicals. *Chem. Sci.* **5**, 3814-3822 (2014).

8 Jensen, K. M. Ø. *et al.* Polymorphism in magic-sized $Au_{144}(SR)_{60}$ clusters. *Nat. Commun.* **7**, 11859 (2016).

9 Chevrier, D. M., Yang, R., Chatt, A. & Zhang, P. Bonding properties of thiolate-protected gold nanoclusters and structural analogs from X-ray absorption spectroscopy. *Nanotechno.l Rev.* **4**, 193-206 (2015).

10 Chevrier, D. M., Zeng, C. J., Jin, R. C., Chatt, A. & Zhang, P. Role of Au_4 units on the electronic and bonding properties of $Au_{-28}(SR)_{20}$ nanoclusters from X-ray spectroscopy. *J. Phys. Chem. C* **119**, 1217-1223 (2015).

11 Jin, R. Quantum sized, thiolate-protected gold nanoclusters. *Nanoscale* **2**, 343-362 (2010).

12 Tsukuda, T. & Häkkinen, H. *Protected metal clusters: From fundamentals to applications* (Elsevier, 2015).

13 Wang, Y. *et al.* Atomically precise alkynyl-protected metal nanoclusters as a model catalyst: Observation of promoting effect of surface ligands on catalysis by metal nanoparticles. *J. Am. Chem. Soc.* **138**, 3278-3281 (2016).

14 Wang, Y. *et al.* Site preference in multimetallic nanoclusters: Incorporation of alkali metal ions or copper atoms into the alkynyl-protected body-centered cubic cluster $[Au_7Ag_8(C{\equiv}C^tBu)_{12}]^+$. *Angew. Chem. Int. Ed.* **55**, 15152-15156 (2016).

15 Wang, Y. *et al.* An intermetallic $Au_{24}Ag_{20}$ superatom nanocluster stabilized by labile ligands. *J. Am. Chem. Soc.* **137**, 4324-4327 (2015).

16 Wan, X. K., Tang, Q., Yuan, S. F., Jiang, D. E. & Wang, Q. M. Au_{19} nanocluster featuring a V-shaped alkynyl-gold motif. *J. Am. Chem. Soc.* **137**, 652-655 (2015).

17 Maity, P., Tsunoyama, H., Yamauchi, M., Xie, S. H. & Tsukuda, T. Organogold clusters protected by phenylacetylene. *J. Am. Chem. Soc.* **133**, 20123-20125 (2011).

18 Weidner, T. *et al.* NHC-based self-assembled monolayers on solid gold substrates. *Aust. J. Chem.* **64**, 1177-1179 (2011).

19 Zhukhovitskiy, A. V., Mavros, M. G., Voorhis, T. V. & Johnson, J. A. Addressable carbene anchors for gold surfaces. *J. Am. Chem. Soc.* **135**, 7418–7421 (2013).

20 Crudden, C. M. *et al.* Ultra stable self-assembled monolayers of N-heterocyclic carbenes on gold. *Nat. Chem.* **6**, 409-414 (2014).

21 Crudden, C. M. *et al.* Simple direct formation of self-assembled N-heterocyclic carbene monolayers on gold and their application in biosensing. *Nat. Commun.* **7**, 12654 (2016).

22 Zhukhovitskiy, A. V., MacLeod, M. J. & Johnson, J. A. Carbene ligands in surface chemistry: From stabilization of discrete elemental allotropes to modification of nanoscale and bulk substrates. *Chem Rev* **115**, 11503-11532 (2015).

23 Larrea, C. R. *et al.* N-heterocyclic carbene self-assembled monolayers on copper and gold: Dramatic effect of wingtip groups on binding, orientation and assembly. *ChemPhysChem* **18**, 3536-3539 (2017).

24 MacLeod, M. J. & Johnson, J. A. Pegylated N-heterocyclic carbene anchors designed to stabilize gold nanoparticles in biologically relevant media. *J. Am. Chem. Soc.* **137**, 7974-7977 (2015).

25 Kim, H. K. *et al.* Reduction of the work function of gold by N-heterocyclic carbenes. *Chem. Mater.* **29**, 3403-3411 (2017).

26 Wang, G. *et al. Nat. Chem.* **9**, 152–156 (2016).

27 Engel, S., Fritz, E. C. & Ravoo, B. J. New trends in the functionalization of metallic gold: From organosulfur ligands to N-heterocyclic carbenes. *Chem. Soc. Re.v* **46**, 2057-2075 (2017).

28 Moller, N. *et al.* Stabilization of high oxidation state upconversion nanoparticles by N-heterocyclic carbenes. *Angew. Chem. Int. Ed.* **56**, 4356-4360 (2017).

29 Salorinne, K. *et al.* Water-soluble N-heterocyclic carbene-protected gold nanoparticles: Size-controlled synthesis, stability, and optical properties. *Angew. Chem. Int. Ed.* **56**, 6198-6202 (2017).

30 Man, R. W. Y. *et al.* Ultrastable gold nanoparticles modified by bidentate N-heterocyclic carbene ligands. *J. Am. Chem. Soc.* **140**, 1576-1579 (2018).

31 Crudden, C. M. & Allen, D. A. Stability and reactivity of N-heterocyclic carbene complexes. *Coord. Chem. Rev.* **248**, 2247-2273 (2004).

32 Hopkinson, M. N., Richter, C., Schedler, M. & Glorius, F. An overview of N-heterocyclic carbenes. *Nature* **510**, 485-496 (2014).

33 Polgar, A. M., Weigend, F., Zhang, A., Stillman, M. J. & Corrigan, J. F. A N-heterocyclic carbene-stabilized coinage metal-chalcogenide framework with tunable optical properties. *J. Am. Chem. Soc.* **139**, 14045-14048 (2017).

34 Azizpoor Fard, M., Levchenko, T. I., Cadogan, C., Humenny, W. J. & Corrigan, J. F. Stable -$ESiMe_3$ complexes of Cu^I and Ag^I (E=S, Se) with NHCs: Synthons in ternary nanocluster assembly. *Chem. Eur. J.* **22**, 4543-4550 (2016).

35 Robilotto, T. J., Bacsa, J., Gray, T. G. & Sadighi, J. P. Synthesis of a trigold monocation: An isolobal analogue of $[H_3]^+$. *Angew. Chem., Int. Ed.* **51**, 12077 –12080 (2012).

36 Khalili Najafabadi, B. & Corrigan, J. F. N-heterocyclic carbenes as effective ligands for the

preparation of stabilized copper- and silver-t-butylthiolate clusters. *Dalton Trans.* **43**, 2104-2111 (2014).
37 McKenzie, L. C., Zaikova, T. O. & Hutchison, J. E. Structurally similar triphenylphosphine-stabilized undecagolds, $Au_{11}(PPh_3)_7Cl_3$ and $[Au_{11}(PPh_3)_8Cl_2]Cl$, exhibit distinct ligand exchange pathways with glutathione. *J. Am. Chem. Soc.* **136**, 13426-13435 (2014).
38 Enkovaara, J. *et al.* Electronic structure calculations with GPAW: A real-space implementation of the projector augmented-wave method. *J. Phys. Condens. Matter* **22**, 253202 (2010).
39 Zhang, P. & Sham, T. K. X-ray studies of the structure and electronic behavior of alkanethiolate-capped gold nanoparticles: The interplay of size and surface effects. *Phys. Rev. Lett.* **90** 245502 (2003).
40 Lopez-Cartes, C. *et al.* Gold nanoparticles with different capping systems: An electronic and structural XAS analysis. *J. Phys. Chem. B* **109**, 8761-8766 (2005).
41 Tang, Q. & Jiang, D.-E. Comprehensive view of the ligand–gold interface from first principles. *Chem. Mater.* **29**, 6908-6915 (2017).
42 Rodríguez-Castillo, M. *et al.* Reactivity of gold nanoparticles towards N-heterocyclic carbenes. *Dalton Trans.* **43**, 5978-5982 (2014).
43 Tang, Q. *et al.* Lattice-hydride mechanism in electrocatalytic CO_2 reduction by structurally precise copper-hydride nanoclusters. *J. Am. Chem. Soc.* **139**, 9728-9736 (2017).
44 Cao, Z. *et al.* A molecular surface functionalization approach to tuning nanoparticle electrocatalysts for carbon dioxide reduction. *J. Am. Chem. Soc.* **138**, 8120-8125 (2016).
45 Cao, Z. *et al.* Chelating N-heterocyclic carbene ligands enable tuning of electrocatalytic CO_2 reduction to formate and carbon monoxide: Surface organometallic chemistry. *Angew. Chem. Int. Ed.* **57**, 4981-4985 (2018).
46 Gray, H. B. Powering the planet with solar fuel. *Nat. Chem.* **1**, 7 (2009).
47 Liu, M. *et al.* Enhanced electrocatalytic CO_2 reduction via field-induced reagent concentration. *Nature* **537**, 382-386 (2016).
48 Zhang, L., Zhao, Z.-J., & Gong, J. Nanostructured Materials for Heterogeneous Electrocatalytic CO_2 Reduction and their Related Reaction Mechanisms. *Angew. Chem. Int. Ed.* **56**, 11326-11353 (2017).

Acknowledgements
CMC, JHH, and EHS acknowledge the Natural Sciences and Engineering Research Council of Canada (NSERC) and the Canada Foundation for Innovation (CFI) and the Ministry of Research Innovation (MRI) for support in terms of discovery grants and infrastructure grants respectively. KA and PJG thank NSERC for support through the awarding of USRA fellowships. MRN thanks the Ontario Graduate Scholarship program and Queen's University for fellowship support. This work was supported by KAKENHI from the Japan Society for the Promotion of Science (JSPS, 17H03030 and 16K13962 to CMC; 17H01182 to TT), Nanotechnology Platform (Project No.12024046) and the Elements Strategy Initiative for Catalysts & Batteries (ESICB). JSPS and NU are acknowledged for funding of this research through The World Premier International Research Center Initiative (WPI) program. The computational work was supported by the Academy of Finland through HH's Academy Professorship. All computations were done at the Finnish CSC computer center. SK thanks the Väisälä Foundation for a personal PhD study grant. Prof. Kenichiro Itami is thanked for assistance with the preparation of this manuscript.

Author contributions
CMC, PU, MRN and KS designed and carried out the synthesis of the nanoclusters, assisted by KA, PJG, MN, KO and RM. KO and RM optimized the synthetic procedures and purifications and acquired TGA-MS data. Mass spectroscopic analysis was performed and interpreted by ST, RT and TT, including CID MS. Crystallization of **3a** was carried out by MN and ST on a sample prepared and purified by KO. DFT studies including prediction of structure and optical spectra were carried out by SK, SM and HH. EXAFS and XANES studies were carried out and interpreted by JHH and DP. Electrocatalytic studies were performed and interpreted by C-TD and EHS. The manuscript was written by CMC with assistance from co-authors.

Additional information
Supplementary information and chemical compound information are available in the online version of the paper. Correspondence and requests for materials should be addressed to CMC, TT or HH.

Competing financial interests
The authors declare no competing financial interests.

Table of Contents Graphical Image

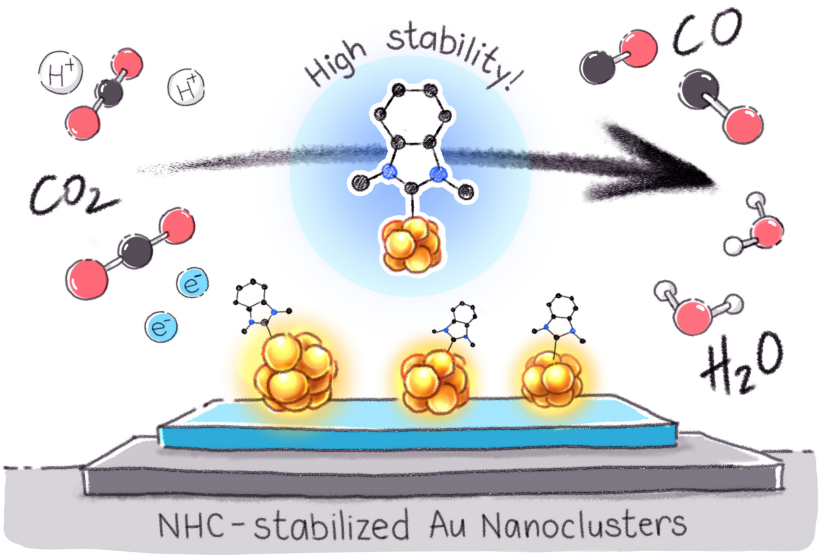
High stability!
CO
CO2
H2O
NHC-stabilized Au Nanoclusters